

S1 WRF-Chem model general description and configuration

In this study, a specific version of the WRF-Chem model (Grell et al., 2005) with modified by Li et al. (2010; 2011a; 2011b; 2012) is used to quantitatively estimate the radiative effect of brown carbon in the NCP. The model was run at a horizontal resolution of 6km with 35 vertical levels, and configured with a single domain (no nesting) of 300×300 grid cells centered at grid point at latitude of 38.0 N and longitude of 116.0 W as shown in Table S1. The model contains a new flexible gas phase chemical module which utilized with SAPRC chemistry mechanism based on the available emission inventory in the present study. The gas-phase chemistry is solved by an Eulerian backward Gauss-Seidel iterative technique with a number of iterations, inherited from NCAR-HANK (Hess et al., 2000).

For the aerosol simulations, the CMAQ/models3 aerosol module (AERO5) developed by US EPA has incorporated into the model (Binkowski and Roselle, 2003). The particle size distribution is represented as the superposition of three lognormal modes. The processes of coagulation, particles growth by the addition of mass, and new particle formation are included. The wet deposition follows the method in the CMAQ module and the dry deposition of chemical species is parameterized following Wesely (1989). The photolysis rates are calculated using the Fast Tropospheric Ultraviolet and Visible (FTUV) Radiation Model ((Tie, 2003; Li et al., 2005) , with the aerosol and cloud effects on the photochemistry (Li et al., 2011a). The inorganic aerosols is predicted with ISORROPIA (version 1.7) (Nenes et al., 1998) which calculates the thermodynamic equilibrium between the ammonia-sulfate-nitrate-chloride-water aerosols and their gas phase precursors of H₂SO₄-HNO₃-NH₃-HCl-water vapor.

The organic aerosol (OA) module is based on the volatility basis-set (VBS) approach with aging (Li et al., 2011b). The primary organic aerosol (POA) are assumed semi-volatile and photochemically reactive (Robinson et al., 2007) and distributed in logarithmically spaced volatility bins. Nine surrogate species are used for POA components followed by Shrivastava et al. (2008) with saturation concentrations (C*) ranging from 10⁻² to 10⁶ μg m⁻³ at room temperature. The secondary organic aerosol (SOA) formation from each anthropogenic or biogenic precursor is calculated using four semi-volatile VOCs with effective saturation concentrations of 1, 10, 100, and 1000 μg m⁻³ at 298 K. The SOA formation via the heterogeneous reaction of glyoxal and methylglyoxal is parameterized as a first-order irreversible uptake by aerosol particles with an uptake coefficient of 3.7×10⁻³ (Liggio, 2005; Zhao et al.,

2006; Volkamer et al., 2007). The OA module has reasonably reproduced the POA and SOA concentration against measurements, and detailed model performance can be found in Li et al. (2011b), Feng et al. (2016), and Xing et al. (2019).

Table S1 WRF-Chem model configurations.

Parameter	Configuration
Regions	The North China Plain (NCP)
Simulation period	January 1 to 30, 2014
Domain size	300 × 300
Domain center	38.0°N, 116.0°E
Horizontal resolution	6km × 6km
Vertical resolution	35 vertical levels with a stretched vertical grid with spacing ranging from 30m near the surface, to 500m at 2.5km and 1km above 14km
Microphysics scheme	WSM 6-class graupel scheme (Hong and Lim, 2006)
Boundary layer scheme	MYJ TKE scheme (Janjić, 2002)
Surface layer scheme	MYJ surface scheme (Janjić, 2002)
Land-surface scheme	Unified Noah land-surface model (Chen and Dudhia, 2001)
Long-wave radiation scheme	Goddard longwave scheme (Chou et al., 2001)
Short-wave radiation scheme	Goddard shortwave scheme (Chou and Suarez, 1999)
Meteorological boundary and initial conditions	NCEP 1°×1° reanalysis data
Chemical initial and boundary conditions	MOZART 6-hour output (Horowitz et al., 2003)
Anthropogenic emission inventory	SAPRC-99 chemical mechanism emissions developed by Zhang et al. (2009) and Li et al. (2017)
Biogenic emission inventory	MEGAN model developed by Guenther et al. (2006)
Four-dimension data assimilation	NCEP ADP Global Air Observational Weather Data
Model spin-up time	24 hours

S2 Data and methodology

S2.1 Observation data description

The hourly near-surface measurements of O₃, NO₂, SO₂, CO and PM_{2.5} concentrations have been released in public by the Ministry of Ecology and Environment of China since 2013. The submicron sulfate, nitrate, ammonium, elemental carbon and organic aerosols obtained in two cities including Beijing, Tianjin and the hourly observation of primary OA from, BB, RCC and motor vehicles emissions and SOA in Beijing in January, 2014 are provided by Institute of Earth Environment, Chinese Academy of Sciences. The organic carbon and elemental carbon concentrations are measured using a thermal/optical reflectance carbon analyzer (Model 2001, DRI, USA) (Chow et al., 2004) and water-soluble ions are measured using a DX600 ion chromatograph (Dionex Inc., Sunnyvale, CA, USA)

(Zhang et al., 2011). The SWDOWN is measured by CM-11 pyranometers at five sites from Chinese Ecosystem Research Network (CERN) in the NCP, including Beijing, Tianjin, Zhengzhou, Hefei, and Ji'nan. The hourly measurement of OA in Beijing is measured by the Aerodyne high-resolution time-of-flight aerosol mass spectrometer (HR-ToF-AMS) with a PM_{2.5} lens from 9 to 25 January, 2014 at the Institute of Remote Sensing and Digital Earth, Chinese Academy of Sciences (Li et al., 2018). The positive matrix factorization (PMF) method is used to distinguish the sources of OA as hydrocarbon-like OA, biomass burning OA, coal combustion OA (Elser et al., 2016), which are interpreted for surrogates of primary OA (POA)-TRA, POA-BB, POA-COAL, and oxygenated OA is the surrogate of SOA in this paper.

S2.2 Statistical metrics for simulation comparisons

In this study, the mean bias (MB), root mean square error (RMSE) and the index of agreement (IOA) are used to evaluate the model performance in simulating air pollutants.

$$MB = \frac{1}{N} \sum_{i=1}^N (P_i - O_i) \quad (1)$$

$$RMSE = \left[\frac{1}{N} \sum_{i=1}^N (P_i - O_i)^2 \right]^{\frac{1}{2}} \quad (2)$$

$$IOA = 1 - \frac{\sum_{i=1}^N (P_i - O_i)^2}{\sum_{i=1}^N (|P_i - \bar{O}| + |O_i - \bar{O}|)^2} \quad (3)$$

Where P_i and O_i are the simulated and observed variables, respectively. N is the total number of the simulations for comparisons, and \bar{O} donates the average of the observations. The IOA ranges from 0 to 1, with 1 showing a perfect agreement of the simulations with the observations.

S3 Model performance

S3.1 Air pollutants simulations in the NCP

Comparison of observed (black dots) and simulated (solid dark blue lines) near-surface hourly mass concentrations of (a) PM_{2.5}, (b) O₃, (c) NO₂, (d) SO₂, and (e) CO averaged at available monitoring sites in the NCP from January 1 to January 30, 2014 is shown in Fig. S1. The model successfully reproduces the diurnal variation of near-surface PM_{2.5} concentrations in the NCP with an IOA of 0.92 and a slightly overestimation with a MB of 3.8 µg m⁻³. The model generally captures well the temporal variations of near-surface O₃ concentrations compared to observations in the NCP with an IOA of 0.90 while a generally overestimates the O₃ concentrations a MB of 0.6 µg m⁻³. The model also reasonably well yields

the temporal variation of NO₂, SO₂ and CO compared with observation, with IOA and MB of 0.82 and -4.0 μg m⁻³, 0.72 and -13.2 μg m⁻³, 0.85 and 0.0 μg m⁻³, respectively.

The spatial pattern of calculated and observed average near-surface concentrations of PM_{2.5}, SO₂, NO₂ and O₃ along with simulated winds in January 2014 in the NCP is shown in Fig. S2. The simulations of four air pollutants distributions are general in good agreement with the observations in the NCP, while partly biases of modeling still exist. It shows that the air in the NCP in January 2014 is much polluted with the monthly near-surface PM_{2.5} concentrations over 150 μg m⁻³. The observed and simulated highest average near-surface PM_{2.5} concentrations are found in Beijing, Hebei, Henan, Shandong, north Anhui and north Jiangsu. Highest observed and simulated near-surface SO₂ and NO₂ concentrations almost occurs in same areas in the NCP. But simulated highest SO₂ concentrations are mainly concentrated around cities, while the distribution of NO₂ shows more area uniformly which likely due to their sources are different, the former mainly emits from point sources and the latter mainly comes from more area sources. The simulated O₃ concentrations are rather low in the NCP which is consistent with measurements.

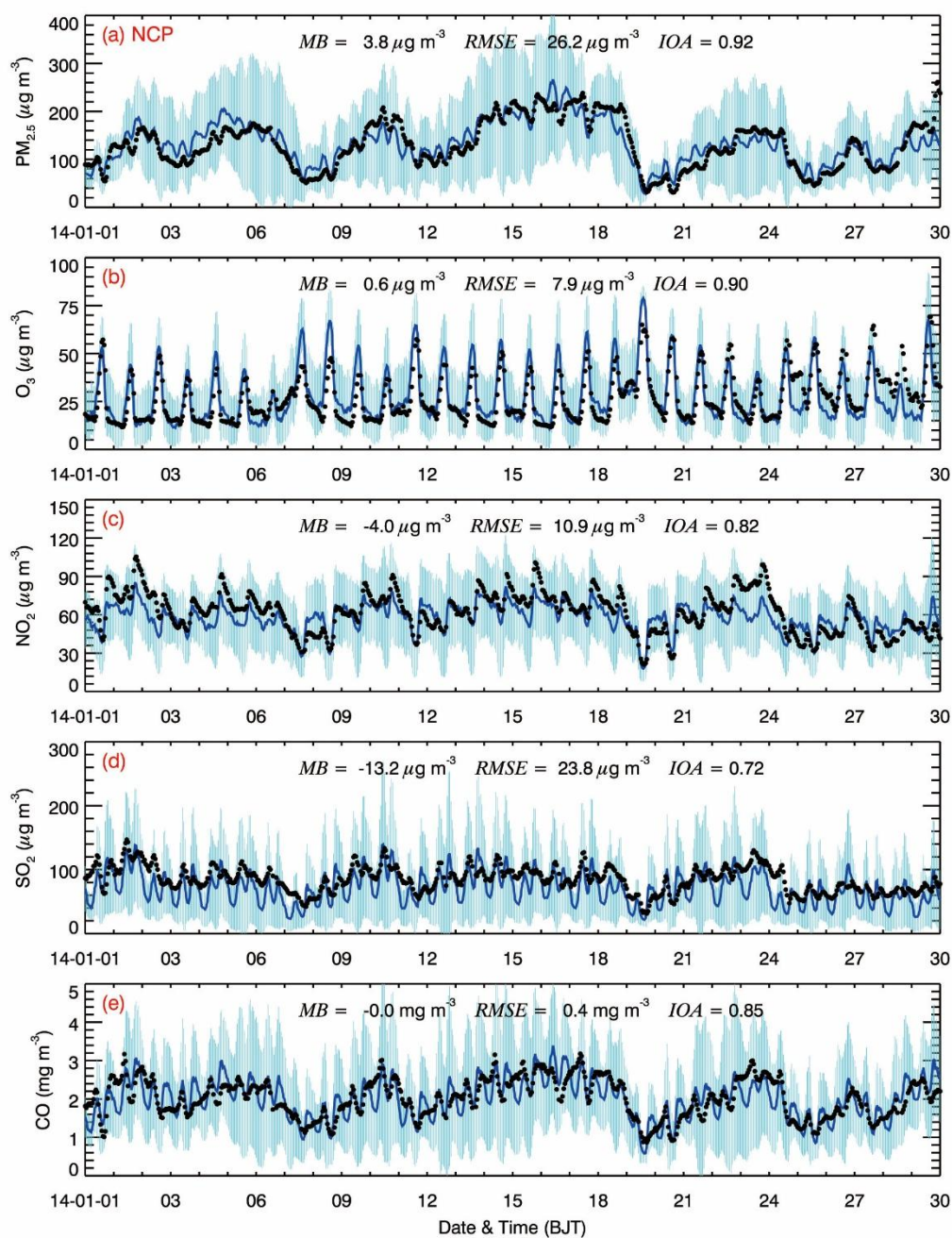


Figure S1. Comparison of observed (black dots) and simulated (dark blue lines) diurnal profiles of near-surface hourly mass concentrations of (a) PM_{2.5}, (b) O₃, (c) NO₂, (d) SO₂, and (e) CO averaged at monitoring sites in the NCP from January 1 to January 30, 2014. The light blue wavy lines represent error bars plotted using standard deviation.

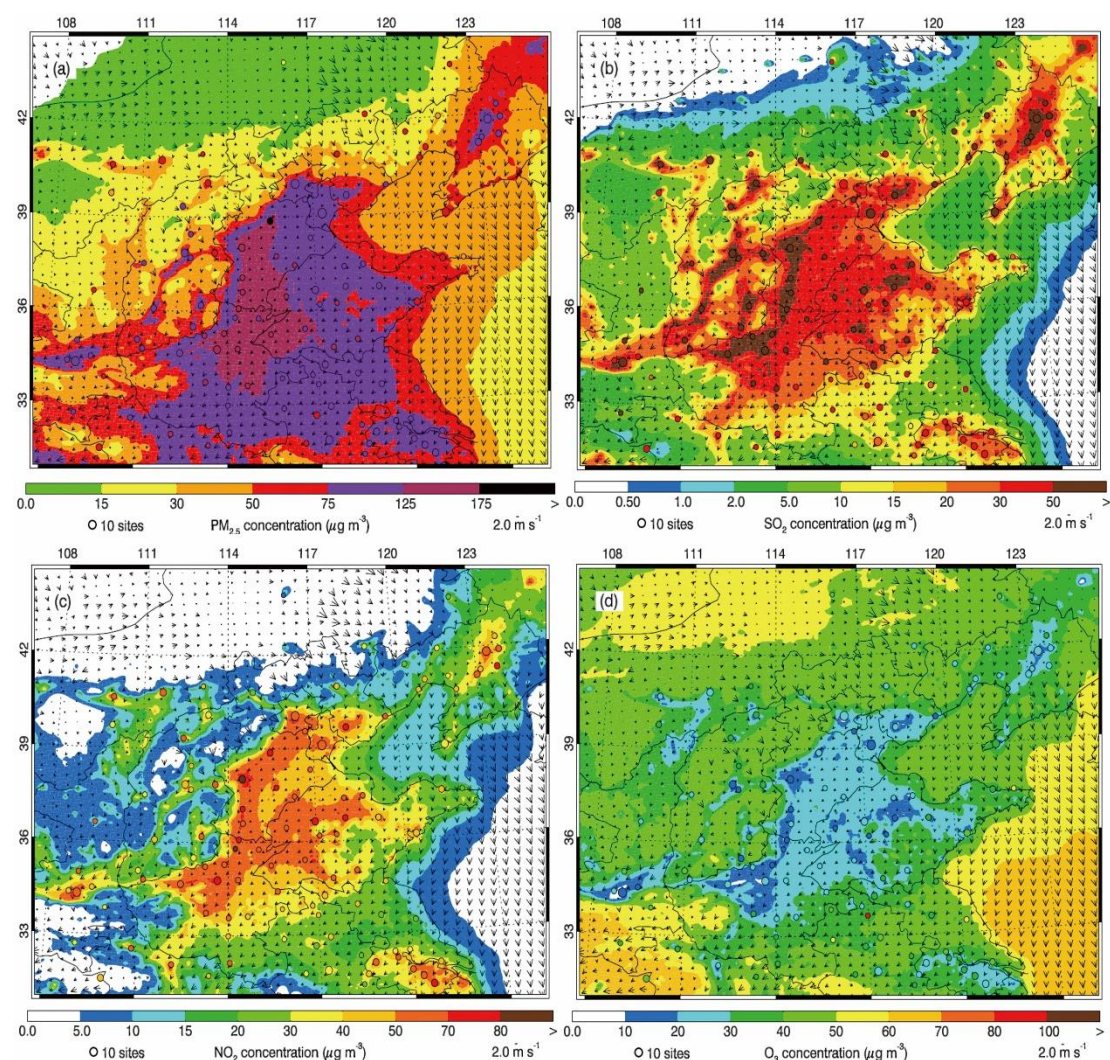


Figure S2. Pattern comparisons of simulated (color counters) vs. observed (colored circles) near-surface mass concentrations of (a) PM_{2.5}, (b) SO₂, (c) NO₂, and (d) O₃ averaged in January 2014. The black arrows indicate simulated surface winds.

Figure S3 provides the time series variations of simulated and observed aerosol species including OA (1.6 times of measurement OC), EC, ammonium, sulfate, and nitrate at Beijing and Tianjin city from January 1 to January 30, 2014. It shows that the WRF-Chem model generally predicts the temporal variations of the aerosol species against the field measurements reasonably with relatively high IOA value. The model yields the main peaks of aerosol species but with some frequently underestimates or overestimates which is mostly linked to the uncertainty of emission inventory and meteorological variations.

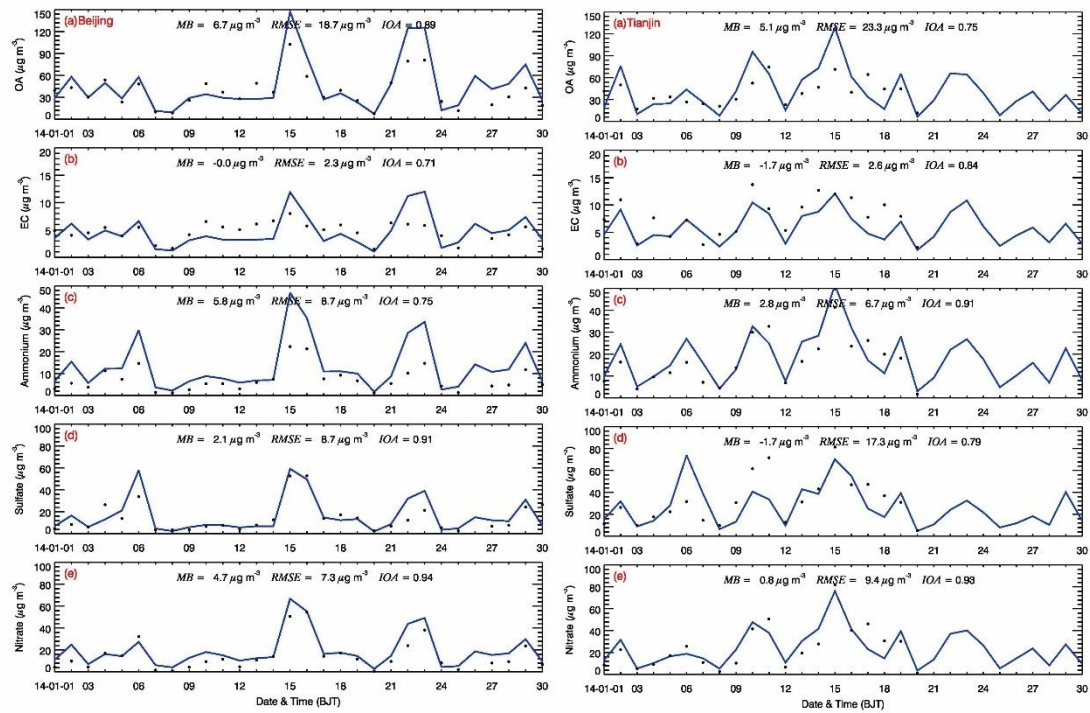


Figure S3. Comparison of measured (black dots) and simulated (blue lines) daily profiles of submicron aerosol species of (a) OA, (b) EC, (c) ammonium, (d) sulfate, and (e) nitrate at two sites (Beijing and Tianjin) in the NCP from January 1 to January 30, 2014.

S3.2 Downward shortwave flux comparison

Figure S4 shows the comparison of measured (black dots) and simulated (blue lines) diurnal profiles of the SWDOWN reaching the ground surface in (a) Beijing, (b) Tianjin, (c) Zhengzhou, (d) Hefei, and (e) Ji'nan from 01 January 2014 to 30 January 2014. Although the MB and RMSE values suggest bias in the model performance, but in overall, the model generally captures the diurnal patterns quite well, as reflected by the average IOA values up to 0.95 across all five cities. The biases of SWDOWN between model and field study may be caused by the cloud cover and optical thickness calculation in the model, which is due to the horizontal resolution of the model is insufficient to resolve the cumulus clouds.

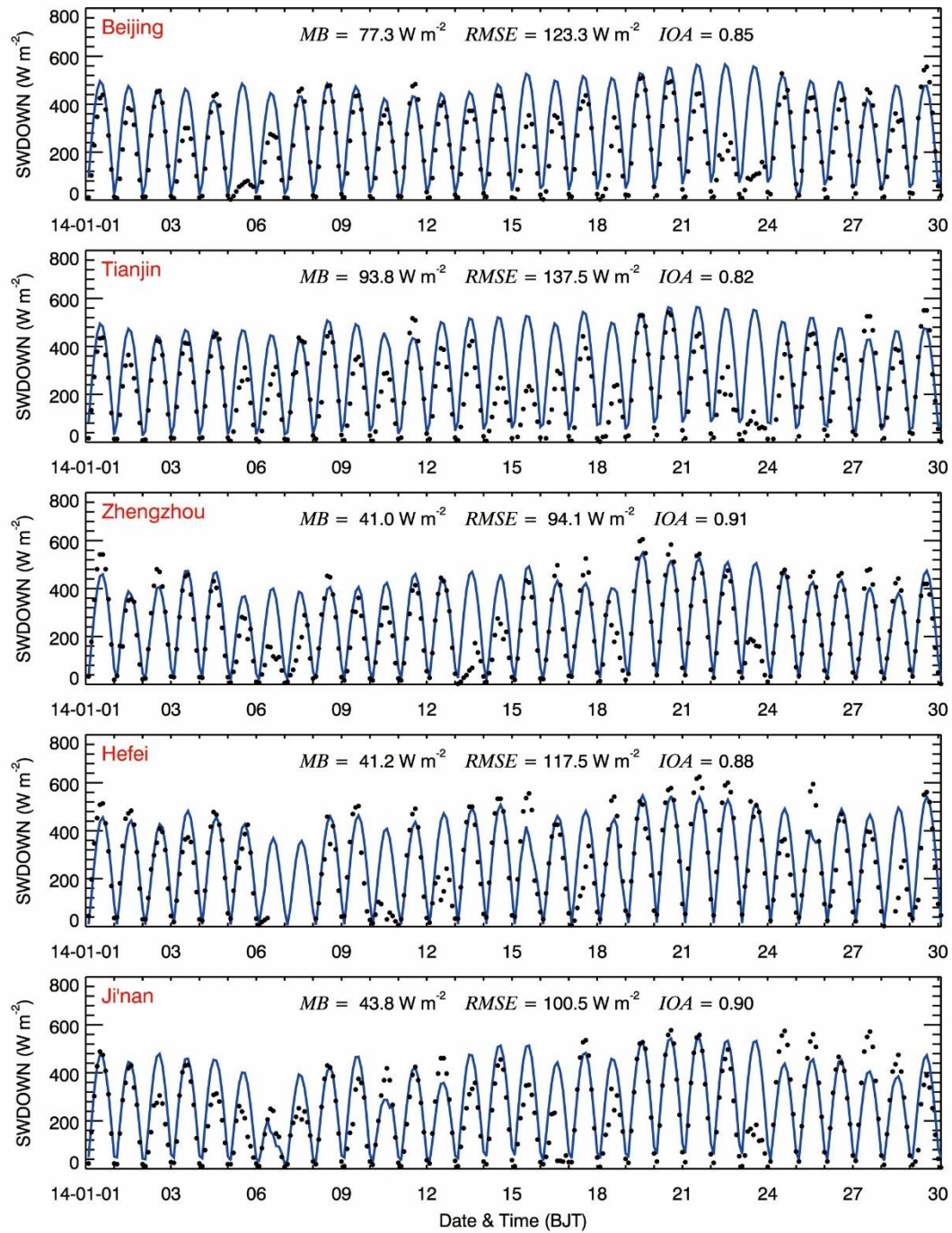


Figure S4. Comparison of measured (black dots) and simulated (blue lines) diurnal profiles of the SWDOWN reaching the ground surface in (a) Beijing, (b) Tianjin, (c) Zhengzhou, (d) Hefei, and (e) Ji'nan from January 1 to January 30, 2014.

S3.3 OA from different sources comparison in Beijing

Figure S5 presents a comparative analysis of temporal profiles of measured and simulated OA, POA from coal combustion (POA-COAL), biomass burning combustion (POA-BB), POA from vehicle exhaust (POA-TRA) and SOA in Beijing from January 9 to 25, 2014. The model shows a good fit with

observed data with an IOA of 0.85, suggesting a reasonably accurate representation of OA variations, despite some discrepancies in peak values and slightly overestimates as indicated by an RMSE of 33.1 $\mu\text{g}/\text{m}^3$ and an MB of 5.0 $\mu\text{g}/\text{m}^3$, respectively. The model also generally tracks the measured diurnal variations in POA-COAL mass concentrations, with an IOA of 0.81. The model frequently underestimates or overestimates the POA-COAL mass concentrations and is also subject to missing the observed POA-COAL peaks. The POA-COAL is mainly emitted from industries and residential coal combustion. In general, the POA-COAL emissions from industries have clear diurnal variations but are opposite for those from residential coal combustion, causing large model biases for the POA-COAL simulation. The model performs well in capturing the general trend of POA-BB with an IOA of 0.86 and a lower RMSE of 4.0 $\mu\text{g}/\text{m}^3$, while POA-Tra has a lower IOA of 0.56. Although the model captured the major vehicle pollution events, some smaller peaks were not well reflected in the model. Modeled SOA shows a fair correlation with observed data (IOA of 0.73) but also exhibits some of the higher variance in peak concentrations, reflected in an RMSE of 11.3 $\mu\text{g}/\text{m}^3$. In general, the IOA values of all types of OA suggest a reasonable model performance, particularly in capturing the temporal dynamics with some quantitative in accuracies which largely associated with the influence of meteorological conditions and emission sources uncertainties.

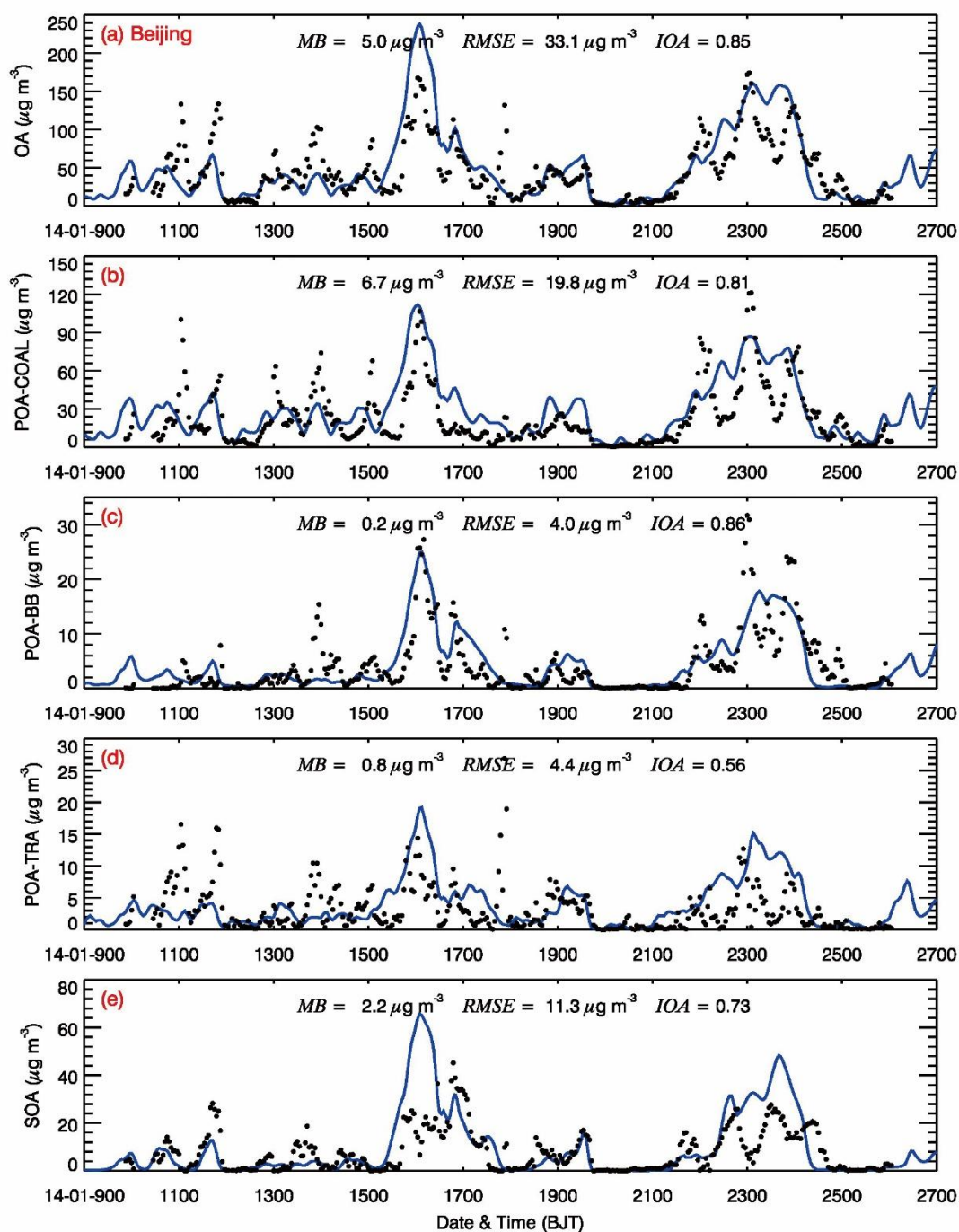


Figure S5. Temporal profiles of measured (black dots) and simulated (blue lines) OA (a), POA-Coal (b), POA-BB (c), POA-Tra (d) and SOA (e) in Beijing from January 9 to 25, 2014.

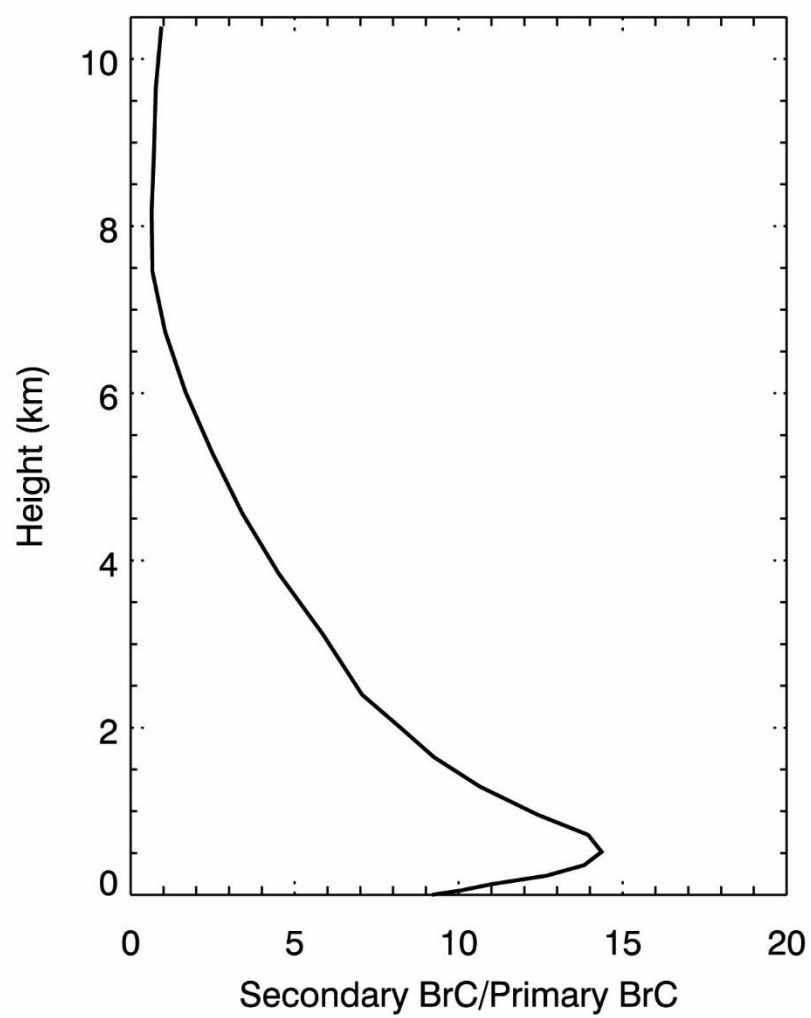


Figure S6. Vertical profile of secondary BrC to primary BrC ratio in NCP in January, 2014

References

- Binkowski, F. S. and Roselle, S. J.: Models-3 Community Multiscale Air Quality (CMAQ) model aerosol component 1. Model description, *J. Geophys. Res.*, 108, 479, <https://doi.org/10.1029/2001JD001409>, 2003.
- Chen, F. and Dudhia, J.: Coupling an Advanced Land Surface–Hydrology Model with the Penn State–NCAR MM5 Modeling System. Part I: Model Implementation and Sensitivity, *Mon. Wea. Rev.*, 129, 569–585, [https://doi.org/10.1175/1520-0493\(2001\)129<0569:CAALSH>2.0.CO;2](https://doi.org/10.1175/1520-0493(2001)129<0569:CAALSH>2.0.CO;2), 2001.
- Chou, M. D. and Suarez, M. J.: A solar radiation parameterization for atmospheric studies, NASA Technique Report, Greenbelt, USA, NASA/TM-1999-104606/VOL15, 1999.
- Chou, M. D., Suarez, M. J., Liang, X. Z., Yan, M. H., and Cote, C.: A Thermal Infrared Radiation Parameterization for Atmospheric Studies, NASA Technique Report, Greenbelt, USA, NASA/TM-2001-104606/VOL19, 2001.
- Chow, J. C., Watson, J. G., Chen, L. W. A., Arnott, W. P., Moosmüller, H., and Fung, K.: Equivalence of elemental carbon by thermal/optical reflectance and transmittance with different temperature protocols, *Environmental science & technology*, 38, 4414–4422, <https://doi.org/10.1021/es034936u>, 2004.
- Elser, M., Huang, R.-j., Wolf, R., Slowik, J. G., Wang, Q., Canonaco, F., Li, G., Bozzetti, C., Daellenbach, K. R., Huang, Y., Zhang, R., Li, Z., Cao, J., Baltensperger, U., El-Haddad, I., and Prévôt, A. S. H.: New insights into PM_{2.5} chemical composition and sources in two major cities in China during extreme haze events using aerosol mass spectrometry, *Atmos. Chem. Phys.*, 16, 3207–3225, <https://doi.org/10.5194/acp-16-3207-2016>, 2016.
- Feng, T., Li, G., Cao, J., Bei, N., Shen, Z., Zhou, W., Liu, S., Zhang, T., Wang, Y., Huang, R.-j., Tie, X., and Molina, L. T.: Simulations of organic aerosol concentrations during springtime in the Guanzhong Basin, China, *Atmos. Chem. Phys.*, 16, 10045–10061, <https://doi.org/10.5194/acp-16-10045-2016>, 2016.
- Grell, G. A., Peckham, S. E., Schmitz, R., McKeen, S. A., Frost, G., Skamarock, W. C., and Eder, B.: Fully coupled “online” chemistry within the WRF model, *Atmospheric Environment*, 39, 6957–6975, <https://doi.org/10.1016/j.atmosenv.2005.04.027>, 2005.
- Guenther, A., Karl, T., Harley, P., Wiedinmyer, C., Palmer, P. I., and Geron, C.: Estimates of global terrestrial isoprene emissions using MEGAN (Model of Emissions of Gases and Aerosols from Nature), *Atmos. Chem. Phys.*, 6, 3181–3210, <https://doi.org/10.5194/acp-6-3181-2006>, 2006.
- Hess, P. G., Flocke, S., Lamarque, J.-F., Barth, M. C., and Madronich, S.: Episodic modeling of the chemical structure of the troposphere as revealed during the spring MLOPEX 2 intensive, *J. Geophys. Res.*, 105, 26809–26839, <https://doi.org/10.1029/2000JD900253>, 2000.
- Hong, S. Y. and Lim, J.O.J.: The WRF single-moment 6-class microphysics scheme (WSM6), *Asia Pacific Journal of Atmospheric Sciences*, 42, 129–151, 2006.
- Horowitz, L. W., Walters, S., Mauzerall, D. L., Emmons, L. K., Rasch, P. J., Granier, C., Tie, X., Lamarque, J.-F., Schultz, M. G., Tyndall, G. S., Orlando, J. J., and Brasseur, G. P.: A global simulation of tropospheric ozone and related tracers: Description and evaluation of MOZART, version 2, *J. Geophys. Res.*, 108, n/a-n/a, <https://doi.org/10.1029/2002JD002853>, 2003.

Janjić, Z. I.: Nonsingular Implementation of the Mellor-Yamada Level 2.5 Scheme in the NCEP Meso Model, 437, Ncep Office Note, Camp Springs, USA, 2002.

Li, G., Lei, W., Bei, N., and Molina, L. T.: Contribution of garbage burning to chloride and PM_{2.5} in Mexico City, *Atmos. Chem. Phys.*, 12, 8751–8761, <https://doi.org/10.5194/acp-12-8751-2012>, 2012.

Li, G., Bei, N., Tie, X., and Molina, L. T.: Aerosol effects on the photochemistry in Mexico City during MCMA-2006/MILAGRO campaign, *Atmos. Chem. Phys.*, 11, 5169–5182, <https://doi.org/10.5194/acp-11-5169-2011>, 2011a.

Li, G., Zavala, M., Lei, W., Tsimpidi, A. P., Karydis, V. A., Pandis, S. N., Canagaratna, M. R., and Molina, L. T.: Simulations of organic aerosol concentrations in Mexico City using the WRF-CHEM model during the MCMA-2006/MILAGRO campaign, *Atmos. Chem. Phys.*, 11, 3789–3809, <https://doi.org/10.5194/acp-11-3789-2011>, 2011b.

Li, G., Lei, W., Zavala, M., Volkamer, R., Dusanter, S., Stevens, P., and Molina, L. T.: Impacts of HONO sources on the photochemistry in Mexico City during the MCMA-2006/MILAGO Campaign, *Atmos. Chem. Phys.*, 10, 6551–6567, <https://doi.org/10.5194/acp-10-6551-2010>, 2010.

Li, G., Zhang, R., Fan, J., and Tie, X.: Impacts of black carbon aerosol on photolysis and ozone, *J. Geophys. Res.*, 110, 1042, <https://doi.org/10.1029/2005JD005898>, 2005.

Li, M., Liu, H., Geng, G., Hong, C., Liu, F., Song, Y., Tong, D., Zheng, B., Cui, H., Man, H., Zhang, Q., and He, K.: Anthropogenic emission inventories in China: a review, *National Science Review*, 4, 834–866, <https://doi.org/10.1093/nsr/nwx150>, 2017.

Li, X., Wu, J., Elser, M., Feng, T., Cao, J., El-Haddad, I., Huang, R., Tie, X., Prévôt, A. S. H., and Li, G.: Contributions of residential coal combustion to the air quality in Beijing–Tianjin–Hebei (BTH), China: a case study, *Atmos. Chem. Phys.*, 18, 10675–10691, <https://doi.org/10.5194/acp-18-10675-2018>, 2018.

Liggio, J.: Reactive uptake of glyoxal by particulate matter, *J. Geophys. Res.*, 110, 881, <https://doi.org/10.1029/2004jd005113>, 2005.

Nenes, A., Pandis, S. N., and Pilinis Christodoulos: ISORROPIA: A New Thermodynamic Equilibrium Model for Multiphase Multicomponent Inorganic Aerosols, *Aquatic Geochemistry*, 4, 123–152, 1998.

Robinson, A. L., Donahue, N. M., Shrivastava, M. K., Weitkamp, E. A., Sage, A. M., Grieshop, A. P., Lane, T. E., Pierce, J. R., and Pandis, S. N.: Rethinking organic aerosols: semivolatile emissions and photochemical aging, *Science* (New York, N.Y.), 315, 1259–1262, <https://doi.org/10.1126/science.1133061>, 2007.

Shrivastava, M. K., Lane, T. E., Donahue, N. M., Pandis, S. N., and Robinson, A. L.: Effects of gas particle partitioning and aging of primary emissions on urban and regional organic aerosol concentrations, *J. Geophys. Res.*, 113, 2701, <https://doi.org/10.1029/2007jd009735>, 2008.

Tie, X.: Effect of clouds on photolysis and oxidants in the troposphere, *J. Geophys. Res.*, 108, 23,073, <https://doi.org/10.1029/2003JD003659>, 2003.

Volkamer, R., San Martini, F., Molina, L. T., Salcedo, D., Jimenez, J. L., and Molina, M. J.: A missing sink for gas-phase glyoxal in Mexico City: Formation of secondary organic aerosol, *Geophys. Res. Lett.*, 34, 641, <https://doi.org/10.1029/2007GL030752>, 2007.

Wesely, M. L.: Parameterization of surface resistances to gaseous dry deposition in regional-scale

numerical models, *Atmospheric Environment* (1967), 23, 1293–1304, [https://doi.org/10.1016/0004-6981\(89\)90153-4](https://doi.org/10.1016/0004-6981(89)90153-4), 1989.

Xing, L., Wu, J., Elser, M., Tong, S., Liu, S., Li, X., Liu, L., Cao, J., Zhou, J., El-Haddad, I., Huang, R., Ge, M., Tie, X., Prévôt, A. S. H., and Li, G.: Wintertime secondary organic aerosol formation in Beijing–Tianjin–Hebei (BTH): Contributions of HONO sources and heterogeneous reactions, *Atmos. Chem. Phys.*, 19, 2343–2359, <https://doi.org/10.5194/acp-19-2343-2019>, 2019.

Zhang, Q., Streets, D. G., Carmichael, G. R., He, K. B., Huo, H., Kannari, A., Klimont, Z., Park, I. S., Reddy, S., Fu, J. S., Chen, D., Duan, L., Lei, Y., Wang, L. T., and Yao, Z. L.: Asian emissions in 2006 for the NASA INTEX-B mission, *Atmos. Chem. Phys.*, 9, 5131–5153, <https://doi.org/10.5194/acp-9-5131-2009>, 2009.

Zhang, T., Cao, J. J., Tie, X. X., Shen, Z. X., Liu, S. X., Ding, H., Han, Y. M., Wang, G. H., Ho, K. F., Qiang, J., and Li, W. T.: Water-soluble ions in atmospheric aerosols measured in Xi'an, China: Seasonal variations and sources, *Atmospheric Research*, 102, 110–119, <https://doi.org/10.1016/j.atmosres.2011.06.014>, 2011.

Zhao, J., Levitt, N. P., Zhang, R., and Chen, J.: Heterogeneous reactions of methylglyoxal in acidic media: Implications for secondary organic aerosol formation, *Environmental science & technology*, 40, 7682–7687, <https://doi.org/10.1021/es060610k>, 2006.